

Title	Bandgap shift by quantum confinement effect in <100> Si-nanowires derived from threshold-voltage shift of fabricated metal-oxide-semiconductor field effect transistors and theoretical calculations
Author(s)	Yoshioka, Hironori; Morioka, Naoya; Suda, Jun; Kimoto, Tsunenobu
Citation	JOURNAL OF APPLIED PHYSICS (2011), 109(6)
Issue Date	2011-03-15
URL	http://hdl.handle.net/2433/160640
Right	Copyright 2011 American Institute of Physics. This article may be downloaded for personal use only. Any other use requires prior permission of the author and the American Institute of Physics. The following article appeared in JOURNAL OF APPLIED PHYSICS 109, 064312 (2011) and may be found at http://link.aip.org/link/?jap/109/064312
Type	Journal Article
Textversion	publisher

Bandgap shift by quantum confinement effect in 100 Si-nanowires derived from threshold-voltage shift of fabricated metal-oxide-semiconductor field effect transistors and theoretical calculations

Hironori Yoshioka, Naoya Morioka, Jun Suda, and Tsunenobu Kimoto

Citation: *J. Appl. Phys.* **109**, 064312 (2011); doi: 10.1063/1.3559265

View online: <http://dx.doi.org/10.1063/1.3559265>

View Table of Contents: <http://jap.aip.org/resource/1/JAPIAU/v109/i6>

Published by the [American Institute of Physics](#).

Related Articles

Band gap enhancement of glancing angle deposited TiO₂ nanowire array
J. Appl. Phys. **112**, 054315 (2012)

Exciton states and oscillator strengths in a cylindrical quantum wire with finite potential under transverse electric field
J. Appl. Phys. **112**, 033715 (2012)

Effect of the energy dependence of the carrier scattering time on the thermoelectric power factor of quantum wells and nanowires
Appl. Phys. Lett. **100**, 242106 (2012)

Exciton confinement and trapping dynamics in double-graded-bandgap quantum nanowires
Appl. Phys. Lett. **100**, 211907 (2012)

Tantalum nitride superconducting single-photon detectors with low cut-off energy
Appl. Phys. Lett. **100**, 062601 (2012)

Additional information on *J. Appl. Phys.*


Journal Homepage: <http://jap.aip.org/>

Journal Information: http://jap.aip.org/about/about_the_journal

Top downloads: http://jap.aip.org/features/most_downloaded

Information for Authors: <http://jap.aip.org/authors>

ADVERTISEMENT



Special Topic Section:
PHYSICS OF CANCER

Why cancer? Why physics? [View Articles Now](#)

Bandgap shift by quantum confinement effect in $\langle 100 \rangle$ Si-nanowires derived from threshold-voltage shift of fabricated metal-oxide-semiconductor field effect transistors and theoretical calculations

Hironori Yoshioka,^{1,a)} Naoya Morioka,¹ Jun Suda,¹ and Tsunenobu Kimoto^{1,2}

¹Department of Electronic Science and Engineering, Kyoto University, Kyoto 615-8510, Japan

²Photonics and Electronics Science and Engineering Center, Kyoto University, Kyoto 615-8510, Japan

(Received 6 November 2010; accepted 22 January 2011; published online 23 March 2011)

Si-nanowire (Si-NW) MOSFETs, the cross-sectional size (square root of the cross-sectional area of NWs) of which was changed from 18 to 4 nm, were fabricated and characterized. Both n- and p-channel MOSFETs have shown a nearly ideal subthreshold swing of 63 mV/decade. The threshold voltage of n-/p-channel MOSFETs has gradually increased/decreased with decreasing the cross-sectional size. The bandgap shift from bulk Si has been derived from the threshold-voltage shift. The bandgap of Si-NWs was calculated by a density functional theory, tight binding method, and effective mass approximation. The calculated bandgap shows good agreement with that derived from threshold voltage. The theoretical calculation indicates that the bandgap is dominated by the cross-sectional size (area) and is not very sensitive to the shape within the aspect-ratio range of 1.0-2.5. © 2011 American Institute of Physics. [doi:10.1063/1.3559265]

I. INTRODUCTION

Si complementary metal-oxide-semiconductor (CMOS) technology has been making great progress due to the scalability of the metal-oxide-semiconductor field effect transistors (MOSFETs). However, further scaling will face severe difficulty in the future,¹⁻³ and Si-nanowire (Si-NW) MOSFETs⁴⁻⁷ are one of the promising candidates for breaking the limits of conventional devices because they can effectively suppress the short-channel effects. In the real application of Si-NW MOSFETs, the cross-sectional size of the NW channel will reach several nanometers where quantum confinement effects will emerge and affect the device characteristics. Therefore it is important to control and utilize quantum confinement effects for enhancing the device performance.

Quantum confinement changes the band structure of materials such as bandgap, effective mass, and density of states. Although all these properties must be clarified by both experimental and theoretical methods, we focus on the bandgap as the first step because the bandgap is a single property and would be easily evaluated. It is theoretically predicted that the bandgap of NWs increases with the decrease of the cross-sectional size,⁸⁻¹³ and it is reported that the bandgap widening changes the threshold voltage of NW MOSFETs.⁵ In previous reports, the threshold-voltage shift is well explained by the bandgap shift qualitatively, but further quantitative analyses are required, taking account of the exact size and cross-sectional shapes. Comparison with theoretical calculation should be also investigated in more detail.

In this study, the bandgap shift in $\langle 100 \rangle$ Si-nanowires with the NW size has been evaluated by threshold-voltage shift of fabricated n- and p-channel MOSFETs and theoretic-

cal calculations of the density functional theory (DFT), tight binding method (TB), and effective mass approximation (EMA). The cross-sectional structure of Si-NWs was measured by TEM for all the MOSFETs characterized in this study. We propose the property of "cross-sectional size," which is defined as the square root of the cross-sectional area of NWs and show that the bandgap is dominated by the cross-sectional size and not very sensitive to the shape.

II. DEVICE STRUCTURE AND FABRICATION

Figure 1 illustrates the schematic structure of the Si-NW MOSFETs fabricated in this study. A Si-NW is connected to both n⁺ and p⁺ regions to evaluate both n- and p-channel MOSFETs in a Si-NW.

The starting material was Si on insulator with the top Si (001) layer with a high resistivity of 5-50 Ω -cm (p-type) and 200-nm-thick buried oxide. The top Si layer was thinned to 37 nm by sacrificial oxidation at 1150 °C. The n⁺/p⁺ region was formed by P/B ion implantation, and implanted dopants were electrically activated during following oxidations. The NW shape was formed by using electron beam lithography and reactive ion etching. The patterning length of the NWs was 100 nm, and the patterning width was changed from 48 to 18 nm, while the NW direction was [100]. To remove the etching damage and to reduce the NW size, sacrificial oxidation was carried out at 1000 °C for 8 min in dry O₂. The gate insulator of SiO₂ was subsequently formed by oxidation at 1000 °C for 13 min in dry O₂. The thickness of the gate SiO₂ was about 15~20 nm. Al was employed for the gate electrodes. Hydrogen-termination treatment at the SiO₂/Si interfaces was carried out in the forming gas at 450 °C for 10 min. The source and drain electrodes were formed by evaporation of Al/Ti on n⁺ region and Al on p⁺ region followed by sintering at 350 °C.

^{a)}Author to whom correspondence should be addressed. Electronic mail: yoshioka@semicon.kuee.kyoto-u.ac.jp.

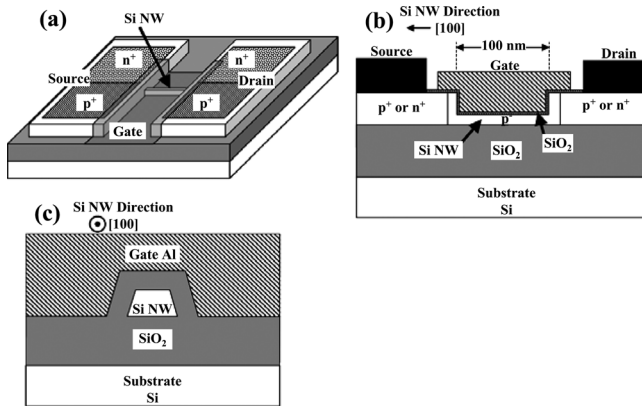


FIG. 1. Schematic structure of the fabricated Si-NW MOSFET: (a) the bird's-eye view, (b) the cross-sectional view parallel to the NW, and (c) the cross-sectional view perpendicular to the NW. The source/drain electrodes and SiO_2 covering Si are omitted in (a).

Figure 2 shows the cross-sectional TEM images of fabricated NWs. The Si-NWs were supported by the buried SiO_2 , and the sides and top of the Si-NW were covered with gate-insulator SiO_2 and gate-electrode Al. The NW cross-sectional shape changed with a change of the patterning

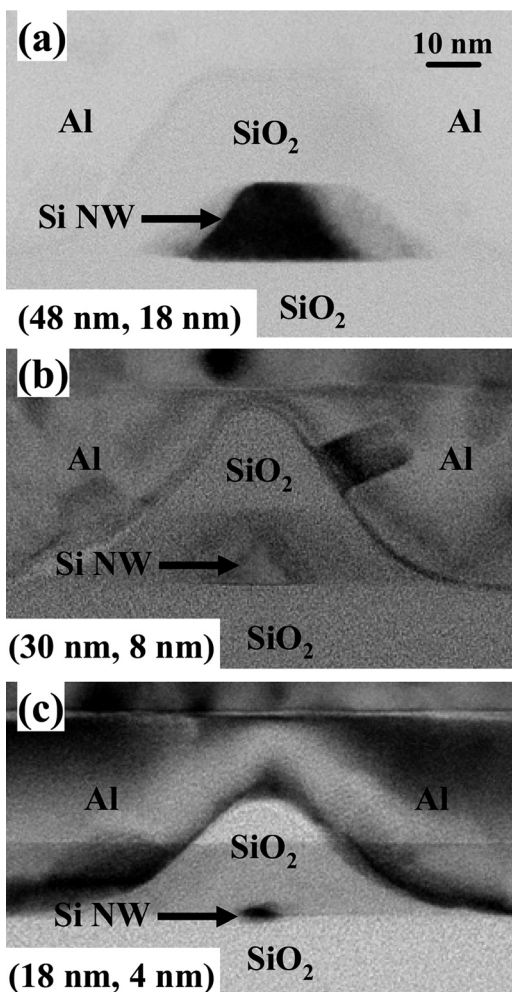


FIG. 2. Cross-sectional TEM images of fabricated Si-NWs with different NW size. The first and second values in the parentheses indicate the patterning width and cross-sectional size (W), respectively.

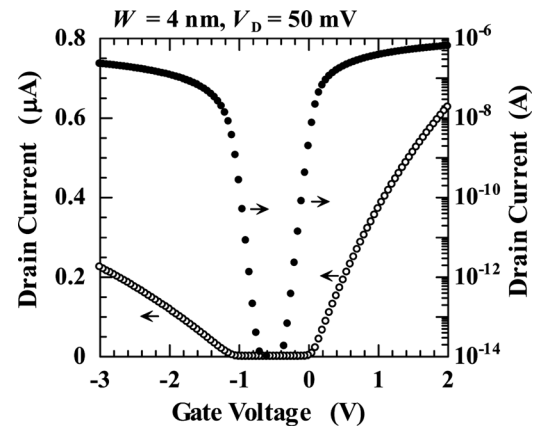


FIG. 3. Gate characteristics (I_D - V_G) of the [100] Si-NW MOSFET with a cross-sectional size (W) of 4 nm at $V_D = 50$ mV and room temperature.

width. To express the size of Si-NWs with different shape, the cross-sectional size (W) of the NWs is defined as the square root of the cross-sectional area determined by the TEM image. The W value gradually decreased from 18 to 4 nm with a decrease in the patterning width from 48 to 18 nm.

III. EXPERIMENTAL RESULTS

Figure 3 shows the drain current (I_D) versus gate voltage (V_G) characteristics for a thin [100] NW MOSFET ($W = 4$ nm) at room temperature. The drain voltage was set at 50 mV, and the substrate voltage was fixed at 0 V. Fabricated MOSFETs worked as both n- and p-channel MOSFETs as intended: the drain current was carried by electrons and holes for $V_G > -0.5$ V and $V_G < -0.5$ V, respectively. MOSFETs also showed good on/off switching with subthreshold current changing exponentially against the gate voltage. The subthreshold swing determined as

$$S \equiv \ln 10 \frac{\partial V_G}{\partial (\ln I_D)} \quad (1)$$

is plotted as a function of the cross-sectional size in Fig. 4. The subthreshold swings of both n- and p-channel MOSFETs

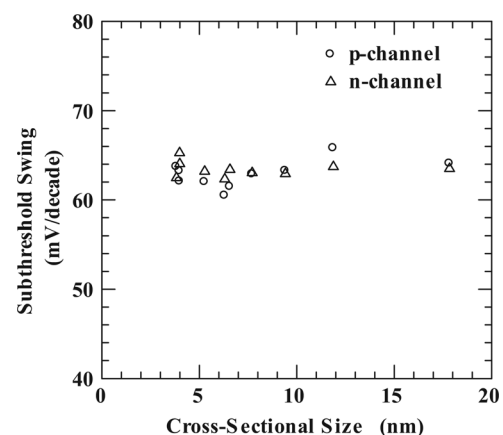


FIG. 4. Cross-sectional size (W) dependence of the subthreshold swing of the [100] Si-NW MOSFETs for n- and p-channel conduction at room temperature.

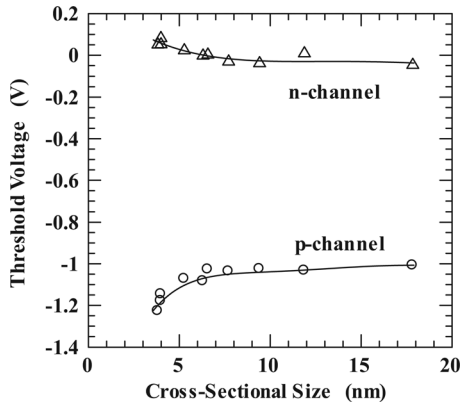


FIG. 5. Cross-sectional size (W) dependence of the threshold voltage for n-channel ($V_{th,e}$) and p-channel ($V_{th,h}$) conduction of the [100] Si-NW MOSFETs.

were about 63 mV/decade and almost unchanged with decrease of the cross-sectional size. The value of 63 mV/decade is very close to the minimum value of 58 mV/decade $[(\ln 10)kT/e]$. The deviation from the minimum value partly originates in a substrate effect. The NW channel is not completely surrounded by the gate electrode, and the bottom part faces the substrate. Taking account of this effect, the ideal subthreshold swing for the present MOSFETs can be estimated to be almost 61 mV/decade.

The threshold voltage ($V_{th,e}/V_{th,h}$) for n/p-channel conduction determined from the linear region of I_D-V_G characteristics is plotted as a function of cross-sectional size in Fig. 5. For MOSFETs with a large W with which the electronic states in the Si-NW channel remain bulk states, $V_{th,e}$ and $V_{th,h}$ were -0.05 and -1.00 V, respectively. The $V_{th,e}/V_{th,h}$ gradually increased/decreased with decreasing the size W . The V_{th} shift must result from the band-edge shift by quantum confinement effect.⁵ Figure 6 schematically illustrates the expected band-edge levels of Si-NWs. The Fermi level at $V_G=0$ in the thick Si-NW should lie slightly below the conduction band minimum [$E_C - E_F(V_G=0) \approx 0.1$ eV] in consideration of the low doping concentration in Si-NWs and the work function difference between Si and gate Al.¹⁴ It is assumed that the energy level of turning-on shifts parallel with the band-edge shift.

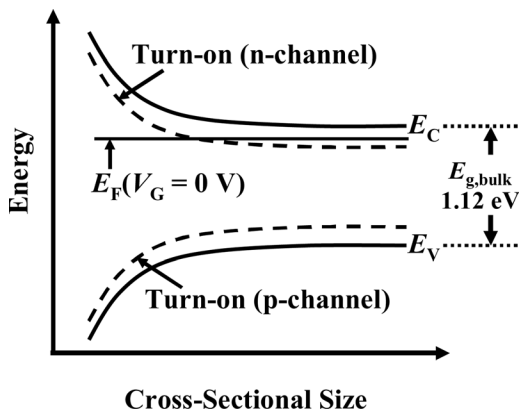


FIG. 6. Schematic illustration of the expected E_C and E_V levels of Si-NWs as a function of cross-sectional size.

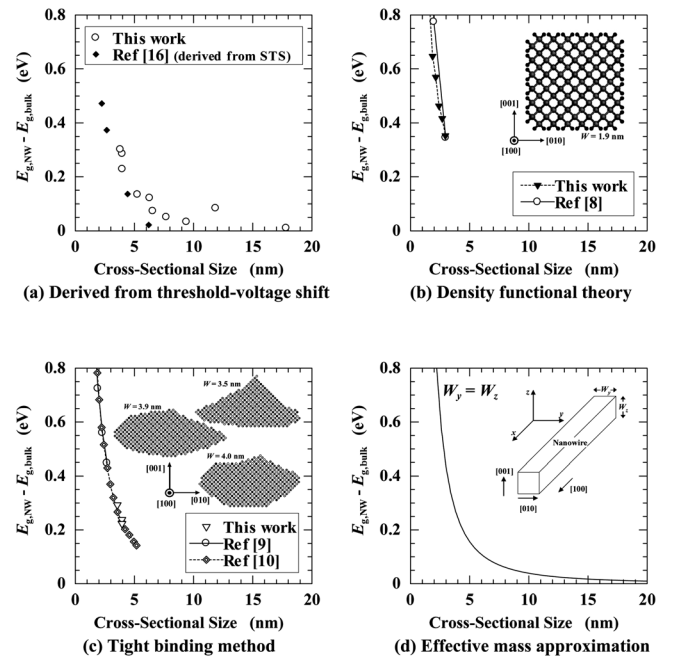


FIG. 7. Cross-sectional size (W) dependence of the bandgap shift of [100] Si-NWs calculated from (a) the threshold-voltage shift of MOSFETs, (b) density functional theory, (c) tight binding method, and (d) effective mass approximation. The bandgaps derived from experimental results of scanning tunneling spectroscopy (STS) by Ma *et al.* (Ref. 16) are also shown in (a).

In the subthreshold region, the change of Fermi level (ΔE_F) in the Si channel is related to the change of gate voltage (ΔV_G) as¹⁵

$$m\Delta E_F = e\Delta V_G, \quad (2)$$

$$m \equiv S \frac{e}{(\ln 10)kT}. \quad (3)$$

Then bandgap shift ($E_{g,NW} - E_{g,bulk}$) is given by

$$m(E_{g,NW} - E_{g,bulk}) = e \left[(V_{th,e} - V_{th,h})_{NW} - (V_{th,e} - V_{th,h})_{bulk} \right] \quad (4)$$

and is plotted in Fig. 7(a) as a function of W , where $(V_{th,e} - V_{th,h})_{bulk}$ was fixed at 0.95 V, which is the value of the MOSFETs with a large W , and m (S) was set at 1.09 (63 mV/decade), which is the average value for all MOSFETs. The bandgap derived from threshold voltage monotonously increased with a W decrease. Although few experimental results of the Si-NW bandgap have been reported so far, Ma *et al.*¹⁶ have derived the bandgap of $\langle 112 \rangle$ or $\langle 110 \rangle$ Si-NWs by scanning tunneling spectroscopy (STS), which are also shown in Fig. 7(a). While the direction of NW is different, the present work showed similar bandgaps to their results for $W < 5$ nm.

IV. METHODS OF THEORETICAL CALCULATION

A. Density functional theory

The bandgap was calculated by the DFT using the CASTEP code,^{17,18} where the gradient corrected exchange-

correlation functional of the Perdew-Burke-Ernzerhof functional (PBE)¹⁹ and the norm-conserving pseudopotentials were adopted. A supercell approach, by which NWs are periodically repeated, was employed. The cutoff energy of the plane wave was set at 200 eV. Although DFT underestimates the bandgap of semiconductors, DFT would well calculate the bandgap change with the size.¹³

As a result of geometrical optimization, the lattice constant (a) of the bulk Si was 0.357 nm. For NWs, Si bond angles (Si-Si-Si) and distances (Si-Si) were fixed to those of the optimized geometry of the bulk Si. All dangling bonds on the surface were terminated by H atoms while maintaining the tetrahedral bond angles and the distance of Si-H bonding (0.154 nm). The precise boundary of NWs at the atomic levels is obscure; this makes it difficult to define the NW volume and cross-sectional size. Then we assume that the average occupation volume of one valence electron in Si-NWs is the same as that of bulk Si ($V_e = a^3/32$), and the cross-sectional size of NWs (W) is defined as

$$W = \sqrt{N_e \times V_e \times \frac{1}{L}}, \quad (5)$$

$$N_e \equiv 4N_{\text{Si}} + N_{\text{H}}, \quad (6)$$

where N_e , N_{Si} , and N_{H} are the number of valence electrons, Si atoms, and H atoms in the unit cell, respectively, L ($=a$) is the edge length of the unit cell in the longitude direction of NWs, and a is the lattice constant of bulk Si. The calculation was performed for square [100] Si-NWs as shown in the inset of Fig. 7(b). The cross-sectional shapes of NWs with different size are similar to those shown in Fig. 7(b), and the space group of NWs was fixed for No. 95 ($D_4^7, P4_322$).

B. Tight binding method

The bandgap of NWs with larger size was calculated by a nearest-neighbor $sp^3d^5s^*$ tight-binding method (TB),²⁰ where the parameters of bulk silicon by Boykin *et al.*²¹ were adopted. The dangling bonds at the surface were pacified by sp^3 hybridization scheme.²² Because this method completely eliminates the electrons at the surface dangling bonds from the valence state, the number of valence electrons in Si-NWs considered in this model becomes

$$N_e \equiv 4N_{\text{Si}} - N_{\text{DB}}, \quad (7)$$

where N_{DB} is the number of dangling bonds. This means that this method may bring a stronger confinement than the explicit hydrogen termination method. Therefore, W is defined by Eqs. (5) and (7) for TB calculation. Si bond angles (Si-Si-Si) and distances (Si-Si) were fixed to those of the bulk Si ($a=0.357$ nm). It is possible for TB to calculate the Si-NW bandgap with the same cross-sectional shape as the fabricated Si-NW MOSFETs. We calculated the bandgap of the three Si-NWs with the cross-sectional shape reproduced from the TEM images of the fabricated Si-NW MOSFETs with a cross-sectional size of about 4 nm [inset of Fig. 7(c)]. The shape of $W=3.9$ nm is a reproduction of the Si-NW shape shown in Fig. 2(c).

C. Effective mass approximation

It is assumed that a Si-NW is rectangular in the cross-section, the crystalline orientations and the coordinate axes are set as shown in the inset of Fig. 7(d), carriers in the Si-NW are confined in the y and z directions by an infinite quantum well of width W_y and W_z ($W_y \geq W_z$), and carriers are free to move in the x direction. To treat the valence band simply, it is roughly assumed that the bands are spherical and parabolic with heavy- and light-hole effective masses. By solving the Schrödinger equation using the EMA, the bandgap shift is given by¹⁵

$$E_{g,\text{NW}} - E_{g,\text{bulk}} = \frac{\hbar^2 \pi^2}{2} \left(\frac{1}{m_{\text{L}}^* W_z^2} + \frac{1}{m_{\text{T}}^* W_y^2} + \frac{1}{m_{\text{H}}^* W_z^2} + \frac{1}{m_{\text{H}}^* W_y^2} \right), \quad (8)$$

where m_{L}^* ($=0.98m_0$) and m_{T}^* ($=0.19m_0$) are the electron longitudinal and transverse effective masses of bulk Si, respectively, and m_{H}^* ($=0.49m_0$) is the heavy hole effective mass.

V. CALCULATION RESULTS AND DISCUSSION

Figures 7(b)–7(d) show the bandgap shift of [100] Si-NWs calculated from DFT, TB, and EMA, respectively. Because DFT requires an extensive amount of calculation capacity, the calculated maximum size was limited to 3.0 nm for a high-symmetrical square shape in this study. The present DFT results are well consistent with those previously reported,⁸ where the cross-sectional shape is slightly different from this work. The size dependence of the bandgap for highly symmetric Si-NWs calculated from TB was reported,^{9,10} which is plotted in Fig. 7(c). The NW shape is a square for Ref. 9 and a circle for Ref. 10 [the radius (R) is converted to the cross-sectional size (W) by $W = \sqrt{R^2 \pi}$ in Fig. 7(c)]. The three results (this work, Ref. 9, and Ref. 10) are well consistent with each other despite the different shape of Si-NWs; this indicates that the bandgap may be dominated by the cross-sectional size (area) and not very sensitive to the shape.

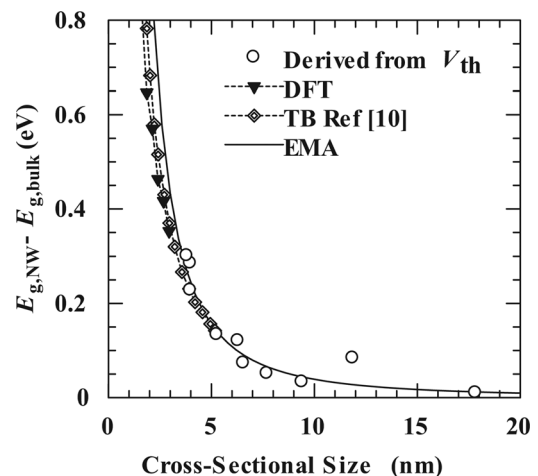


FIG. 8. Comparison of the bandgap shifts derived from the threshold-voltage shift and various calculations. The same data as shown in Fig. 7 are plotted by the same symbols.

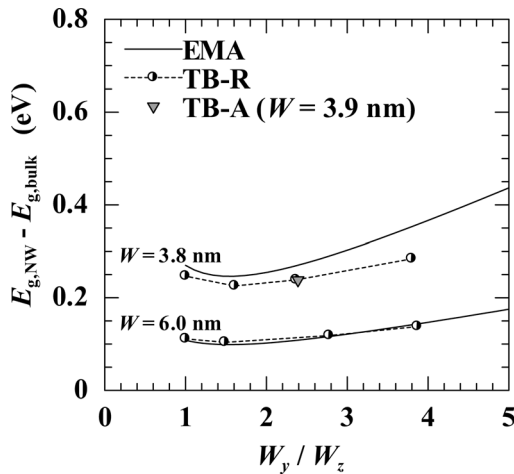


FIG. 9. Aspect ratio (W_y/W_z) dependence of the bandgap shift with a fixed cross-sectional size ($W=3.8$ nm, 6.0 nm). The cross-sectional shape is a rectangle with (010) and (001) sides for effective mass approximation (EMA) and tight binding method (TB-R). The tight-binding result (TB-A) for the shape shown in the inset of Fig. 7(c) ($W=3.9$ nm, $W_{y,max}/W_{z,max}=2.4$) is also shown.

The bandgap shift derived from the threshold-voltage shift, DFT, TB, and EMA is compared in Fig. 8. The bandgap derived from V_{th} shows good agreement with the results of TB and EMA; this indicates that the shift of threshold voltage originates in the band edge shift by quantum confinement effect. The bandgap estimated by EMA is overestimated for thin NWs as indicated,^{11,12} but was almost consistent with the TB results for $W=4\sim 5$ nm, which indicates that the bandgap is reasonably calculated by EMA for a cross-sectional size of more than about 4 nm. The bandgap shifts determined by DFT and TB agree with each other for $W<3$ nm.

It is expected that NWs with a different shape have different bandgaps even though they have the same cross-sectional size. In Figs. 7 and 8, however, NWs with the different shapes are mixed up. Then we tried to verify its validity. Figure 9 shows the aspect ratio (W_y/W_z) dependence of the bandgap shift with a fixed cross-sectional size ($W=3.8$ nm, 6.0 nm). The cross-sectional shape is a rectangle with (010) and (001) sides for EMA and TB (EMA and TB-R in Fig. 9). The TB result for the shape shown in the inset of Fig. 7(c) ($W=3.9$ nm, $W_{y,max}/W_{z,max}=2.4$) is also shown in Fig. 9 (TB-A). The bandgaps of the NWs with $W=3.8$ nm and $W=6.0$ nm show a similar dependence on the aspect ratio (W_y/W_z), and the dependence is rather small within the range of $1.0 \leq W_y/W_z \leq 2.5$. Because the aspect ratio of NWs of fabricated MOSFETs was $1.5\sim 2.4$, evaluation of the bandgap by the cross-sectional size for Si-NWs with different shapes may be valid. The bandgap of EMA shows a similar trend to the TB bandgap with the minimum at about $W_y/W_z=1.6$, which indicates that EMA with the assumption of the simplified valence band can reasonably predict the bandgap change.

VI. CONCLUSIONS

Si-NW MOSFETs, the cross-sectional size (W) of which was changed from 18 to 4 nm, were fabricated and characterized. Both n- and p-channel MOSFETs showed a nearly ideal subthreshold swing of 63 mV/decade. The threshold voltage

of n-/p-channel MOSFETs has gradually increased/decreased with a W decrease. The bandgap shift derived from the threshold-voltage shift of the fabricated Si-NW MOSFETs is well reproduced from the calculation (density functional theory, tight binding method, and effective mass approximation) for the Si-NWs with H termination without strain and surface reconstruction. The calculated results indicate that the bandgap is dominated by the cross-sectional size (area) and not very sensitive to the shape within the aspect-ratio range of 1.0-2.5. Based on the results in this study, one can estimate the cross-sectional size from the threshold-voltage shift without destructive observation of NW shape.

ACKNOWLEDGMENTS

The authors would like to thank Mr. Eiji Ohmura of Kyoto-Advanced Nanotechnology Network, Kyoto University, for supporting us in the device fabrication process of electron beam lithography. The authors appreciate Professor Toshiro Hiramoto, University of Tokyo, for meaningful comments. This work was supported by the Global COE Program (C09) from the Ministry of Education, Culture, Sports, Science and Technology, Japan.

- ¹W. Haensch, E. J. Nowak, R. H. Dennard, P. M. Solomon, A. Bryant, O. H. Dokumaci, A. Kumar, X. Wang, J. B. Johnson, and M. V. Fischetti, *IBM J. Res. Dev.* **50**, 339 (2006).
- ²D. J. Frank, R. H. Dennard, E. Nowak, P. M. Solomon, Y. Taur, and H.-S. P. Wong, *Proc. IEEE* **89**, 259 (2001).
- ³R. W. Keyes, *Rep. Prog. Phys.* **68**, 2701 (2005).
- ⁴N. Singh, A. Agarwal, L. K. Bera, T. Y. Liow, R. Yang, S. C. Rustagi, C. H. Tung, R. Kumar, G. Q. Lo, N. Balasubramanian, and D.-L. Kwong, *IEEE Electron Device Lett.* **27**, 383 (2006).
- ⁵H. Majima, H. Ishikuro, and T. Hiramoto, *IEEE Electron Device Lett.* **21**, 396 (2000).
- ⁶V. Pott, K. E. Moselund, D. Bouvet, L. D. Michielis, and A. M. Ionescu, *IEEE Trans. Nanotechnol.* **7**, 733 (2008).
- ⁷K. H. Cho, S. D. Suk, Y. Y. Yeoh, M. Li, K. H. Yeo, D.-W. Kim, D. Park, W.-S. Lee, Y. C. Jung, B. H. Hong, and S. W. Hwang, *IEEE Electron Device Lett.* **28**, 1129 (2007).
- ⁸T. Vo, A. J. Williamson, and G. Galli, *Phys. Rev. B* **74**, 045116 (2006).
- ⁹Y. Zheng, C. Rivas, R. Lake, K. Alam, T. B. Boykin, and G. Klimeck, *IEEE Trans. Electron Devices* **52**, 1097 (2005).
- ¹⁰Y. M. Niquet, A. Lherbier, N. H. Quang, M. V. Fernández-Serra, X. Blase, and C. Delerue, *Phys. Rev. B* **73**, 165319 (2006).
- ¹¹K. Nehari, N. Cavassilas, J. L. Autran, M. Bescond, D. Munteanu, M. Lannoo, *Solid State Electron.* **50**, 716 (2006).
- ¹²C. Harris and E.P. O'Reilly, *Physica E (Amsterdam)* **32**, 341 (2006).
- ¹³B. Delley and E.F. Steigmeier, *Appl. Phys. Lett.* **67**, 2370 (1995).
- ¹⁴S. M. Sze, *Semiconductor Devices: Physics and Technology* (Wiley, New York, 2002).
- ¹⁵M. S. Lundstrom and J. Guo, *Nanoscale Transistors: Device Physics, Modeling and Simulation* (Springer, New York, 2006).
- ¹⁶D. D. Ma, C. S. Lee, F. C. K. Au, S. Y. Tong, and S. T. Lee, *Science* **299**, 1874 (2003).
- ¹⁷M. D. Segall, P. J. D. Lindan, M. J. Probert, C. J. Pickard, P. J. Hasnip, S. J. Clark, and M. C. Payne, *J. Phys.: Condens. Matter* **14**, 2717 (2002).
- ¹⁸S. J. Clark, M. D. Segall, C. J. Pickard, P. J. Hasnip, M. J. Probert, K. Refson, and M. C. Payne, *Z. Kristallogr.* **220**, 567 (2005).
- ¹⁹J. P. Perdew, K. Burke, and M. Ernzerhof, *Phys. Rev. Lett.* **77**, 3865 (1996).
- ²⁰J.-M. Jancu, R. Scholz, F. Beltram, and F. Bassani, *Phys. Rev. B* **57**, 6493 (1998).
- ²¹T. B. Boykin, G. Klimeck, and F. Oyafuso, *Phys. Rev. B* **69**, 115201 (2004).
- ²²S. Lee, F. Oyafuso, P. von Allmen, and G. Klimeck, *Phys. Rev. B* **69**, 045316 (2004).